High-Resolution Martian Soil Thickness Derived from Yearly Surface Temperatures

by

Simon Heath

A Thesis Presented in Partial Fulfillment
of the Requirement for the Degree
Master of Science

Approved April 2013 by the
Graduate Supervisory Committee:

Philip Christensen, Chair
James Bell
Richard Hervig

ARIZONA STATE UNIVERSITY

May 2013

ABSTRACT

The temperature of a planet's surface depends on numerous physical factors, including thermal inertia, albedo and the degree of insolation. Mars is a good target for thermal measurements because the low atmospheric pressure combined with the extreme dryness results in a surface dominated by large differences in thermal inertia, minimizing the effect of other physical properties. Since heat is propagated into the surface during the day and re-radiated at night, surface temperatures are affected by sub-surface properties down to several thermal skin depths. Because of this, orbital surface temperature measurements combined with a computational thermal model can be used to determine sub-surface structure. This technique has previously been applied to estimate the thickness and thermal inertia of soil layers on Mars on a regional scale, but the Mars Odyssey Thermal Emission Imaging System "THEMIS" instrument allows much higher-resolution thermal imagery to be obtained. Using archived THEMIS data and the KRC thermal model, a process has been developed for creating high-resolution maps of Martian soil layer thickness and thermal inertia, allowing investigation of the distribution of dust and sand at a scale of 100 m/pixel.

ACKNOWLEDGMENTS

First I'd like to thank my graduate committee for all the help they've given me both in my research and in the process of writing my thesis. They have always done their best to make me feel a valued member of the their research groups, and provided swift and useful input on the various problems I've faced. Because of them I'm secure in the knowledge that the work I've done is a valuable contribution to science. I am sure they are as sorry to see me go as I am to leave.

I would also like to thank my colleagues working on related projects at other instiutions for their professionalism and willingness to share their work for the benefit of the entire field. Additionally, the rigorous quality of their results has been truly inspiring.

Finally, I would like to thank Arizona State University and the School of Earth and Space Exploration for their commitment to providing the best and most effective education possible to all of their students, having the highest standards of achievement, and making sure that the facilities and services provided are the best available. The school's devotion to results over appearances ensures that it will always be one of the finest institutions of its kind.

TABLE OF CONTENTS

LIST OF TABLES

LIST OF FIGURES

Chapter 1

INTRODUCTION

No single remote sensing data source can tell everything there is to know about a planet's surface. Instead for most investigations many different types of data are correlated, each one providing pieces of information to be fit together into a larger picture. Thermal remote sensing is useful to Mars exploration because it can provide physical information on the nature of the surface that is not easily obtained by methods such as visible light or ground-penetrating radar. The temperature changes of Mars's surface are governed chiefly by abundance of boulders, grain size and thickness of the soil, and the presence of volatiles such as water and carbon dioxide. Because of this, remote sensing of thermal radiation is an useful tool not only for understanding the nature and processes of Mars's surface, but also for planning future missions, both robotic and manned.

The exploration of Mars's thermal properties originates from telescopic observation (Morrison *et al.*, 1969) and the Mariner spacecraft (Neugebauer *et al.*, 1971), but most modern data has come from three orbital instruments: The Viking Infrared Thermal Mapper (IRTM) (Kieffer *et al.*, 1976; Chase *et al.*, 1978), the Mars Global Surveyor Thermal Emission Spectrometer (TES) (Christensen *et al.*, 1992, 2001), and the Mars Odyssey Thermal Emission Imaging System (THEMIS) (Russell, 2004). The temperature response of a planet's surface is governed by many factors including emissivity, grain size and degree of cementation, and presence of ice or frost. Because of this, surface temperature can provide insight into many processes at many different scales. The IRTM instrument surveyed Mars on a large scale to provide a baseline reference point for more directed investigation, TES included a hyperspectral spec-

trometer, radiometer and bolometer, each with a surface resolution of 3×6 km per pixel, and THEMIS is a high-resolution thermal imager that can provide 100 meter per pixel imagery in 9 distinct spectral bands. Derived properties from these orbital instruments have been calibrated with in-situ observations from landers and rovers, and used as a baseline against which to compare global-scale climate and thermal transfer models. This has allowed orbital temperature measurements to be used for tasks such as estimating abundance of boulders on the surface (Christensen, 1986), detecting sub-surface ice (Bandfield and Feldman, 2008), and mapping the extent of dust cover.

For this work a technique was developed to use THEMIS infrared imaging data combined with surface temperature modeling to derive the thickness of soil layers such as dust and sand on Mars's surface, at a resolution of 100 meters per pixel. The goal is to produce a general-purpose tool suitable for surveying specific sites and features, creating maps of these surface properties using archived THEMIS imagery for the purpose of investigating the properties of Mars's surface on a local rather than regional scale.. This technique has been used with TES data to construct global maps of permafrost depth (Bandfield and Feldman, 2008), and tested using THEMIS (Bandfield, 2007) imagery, but has not been rigorously applied to THEMIS images and used to investigate small-scale features. The model of fine-grained surface cover over a competent layer of rock, permafrost or cemented grains is a good approximation for large areas of Mars's surface, and the results of this technique can be used to investigate the subsurface structure of features such as sand sheets, wind streaks and local temperature anomalies.

Chapter 2

BACKGROUND

Thermal inertia (TI) is an intrinsic property of a planetary surface, describing how rapidly the material stores and conducts heat. It is useful both as an input to global climate models and as a probe into the physical properties of the surface (Putzig *et al.*, 2005; Mellon and Jakosky, 1995). Because of this it is a flexible tool for orbital remote sensing and has been used to study the physical nature of many planetary surfaces.

Thermal inertia is defined as:

$$I = \sqrt{k\rho c}$$

where I is thermal inertia ($\frac{J}{m^2 K\sqrt{\text{sec}}}$; sometimes called tiu, these units are implicit for all following thermal inertia figures), k is thermal conductivity, ρ is density, and c is specific heat at constant pressure. In most geological surfaces on Mars thermal conductivity is the dominant term, varying by several orders of magnitude while density and specific heat vary over a factor of two or three (Wechsler and Glaser, 1965; Neugebauer *et al.*, 1971; Presley and Christensen, 1997a). In the absence of significant water vapor and at a fixed atmospheric pressure, thermal conductivity is governed primarily by the grain size and competency of the surface rather than chemical composition (C. and Price, 1985); because of this thermal inertia can provide information about the physical (as opposed to mineralogical) nature of a planet. Solid rock, permafrost and cemented grains with low porosity have a high thermal inertia (on the order of 1000–2000 $\frac{J}{m^2 K\sqrt{\text{sec}}}$) because they conduct heat efficiently into the

planet, while dust, sand and poorly-consolidated soils act as an insulator resulting in low thermal inertia (20-400). Partially-cemented soils and duricrust range between these extremes, though even a small amount of cementation can significantly increase a surface's TI (Putzig and Mellon, 2007a; Bell, 2008). Effectively this results in high-TI surfaces being relatively cool during the day as absorbed heat is efficiently moved deeper into the surface and warm night as the stored heat is released. Low-TI surfaces on the other hand grow very hot during the day as absorbed heat accumulates in the uppermost surface, which is then released very quickly at night making these materials relatively cool.

This is due to its low but nonzero atmospheric pressure. The mechanisms that conduct heat through an aggregate surface are by grain-to-grain conduction, by emissive radiation and absorbtion between adjacent grains, and by the conduction of heat by the atmosphere filling intergrain pores. This last effect is greater than the other two, and depends on the atmospheric pressure and grain size. On a body such as Mars with very low atmospheric pressure, the size of pores between grains, determined by the size of the grains themselves, has a very strong effect on how efficiently the atmosphere conducts heat between grains.

The scale at which this happens is described by the Knudsen number Kn:

$$Kn = \frac{MFP}{d}$$

Where MFP is the molecular mean free path, the average distance traveled by a molecule of atmosphere before interacting with another one, and d and a physical scale length, in this case the pore size. The mean free path is governed by the cross-section of the gas molecules (which is similar for oxygen, nitrogen and carbon dioxide), the temperature of the gas (which varies by roughly a factor of two over Mars's surface), and the air pressure (which varies by on Mars depending on elevation, season and

local weather). If $Kn \ll 1$, a molecule of atmosphere will almost always interact with another atmosphere molecule before it can travel the length of a pore space. This results in a smooth heat gradient in the gas filling the pore, which operates as predicted by classical heat conduction and efficiently moves energy between grains regardless of grain size; thus, the thermal conductivity of a bulk aggregate is relatively high and only weakly dependent on grain size. If the atmospheric pressure decreases, as Kn approaches 1 there are not enough air molecules to effectively conduct heat in a predictable manner, and so the thermal conductivity of the bulk aggregate decreases, until in a pure vacuum heat flow is entirely via radiation and conduction through grain-to-grain contacts, resulting in a low thermal conductivity which is also only weakly dependent on grain size.

On Mars the atmospheric pressure is low enough for $Kn \approx 1$ for the pore spaces in fine grained dusts (10's of micrometers), while $Kn \ll 1$ for the pore spaces in more coarse materials (100's of micrometers). This creates a very large difference in thermal conductivity based on grain size, since the size of pores determines whether or not the atmosphere helps conduct heat through the aggregate (Presley and Christensen, 1997b,c). This is the reason that Mars's surface exhibits a much wider range of thermal inertias than other bodies such as the Earth or Moon.

The temperature of a planet's surface is partially governed by its subsurface properties. Solar heat can be conducted several meters into the surface and be stored during times of net energy input, only to be conducted out and re-radiated once insolation decreases. Because of this, surface temperature measurements can be used to derive sub-surface properties and structure. The influence of subsurface structure on surface temperature depends on the depth heat is conducted into the surface, described by the thermal skin depth, δ. This thermal skin depth is defined as:

$$\delta = \sqrt{\frac{k}{\rho c}}\sqrt{\frac{P}{\pi}}$$

where P is the period of the temperature change, and all other terms are as above. Analogous to optical or electrical skin depth, thermal skin depth is a measure of how deep into a material a cyclic temperature change (heat pulse) propagates before its magnitude is reduced by a factor of e. A convenient rule of thumb then is that the temperature of a surface is dominated by the thermal properties of the top few skin depths of material. Since the skin depth depends on the period of the temperature cycle, slower cycles have more time to propagate down into the surface, and so penetrate deeper. The thermal properties of Mars have been studied at a variety of skin depths, corresponding to the duration of a Phobos transit (resulting in a skin depth of 0.0001–0.005 meters, depending on surface thermal inertia) (Betts *et al.*, 1995), diurnal cycles (skin depth of 0.03–0.15 meters) (Putzig *et al.*, 2005; Palluconi and Kieffer, 1981), and seasonal cycles (skin depth of 0.05–1.5 meters) (Bandfield and Feldman, 2008). Thus by measuring surface temperatures over the course of a year it is possible to derive properties for a thicker portion of Mars's surface than by using diurnal measurements alone.

The thermal inertia of the Martian surface has been investigated at a variety of spatial resolutions and with different assumptions about the structure of the surface. (Putzig *et al.*, 2005) used thermal measurements from TES to construct a global map of apparent thermal inertia and identify several large-scale units assuming a homogeneous surface. (Bandfield and Feldman, 2008) produced a similar global map using a two-layer model, showing the thermal inertia and thickness of a low-TI soil layer overlying high-TI bedrock or permafrost (which is similar to bedrock in TI; the differences in conductivity, density and heat capacity roughly cancel out). Interpreting the high-TI layer as permafrost at high latitudes this map agrees well with permafrost

depth measurements made by the Mars Odyssey Gamma Ray Spectrometer instrument (Feldman *et al.*, 2007), surface trenching from the Phoenix lander, and computer models of the stability of subsurface ice on Mars (Mellon *et al.*, 1997; Sizemore *et al.*, 2009).

The TES dataset has a coarse spatial resolution of about 3×6 km per pixel. THEMIS can provide surface temperature images with a 100 meter per pixel spatial resolution, with temperature resolution nearly as good as TES. This imaging capability lends it to the study of the physical properties of specific surface features as well as regional scale maps. THEMIS has been used to construct a global thermal inertia map with results roughly comparable to TES, as well as look in greater detail at resolvable surface features such as layered deposits and areas mantled by dust (Fergason *et al.*, 2006). However apart from the Phoenix Lander landing site (Bandfield, 2007) THEMIS has not been used in combination with a layered surface model to examine the subsurface structure of smaller-scale features.

Interestingly, Joachim Audouard of Universit Paris-Sud is currently working on the same task, creating high-resolution maps of soil cover thickness and TI using the Observatoire pour la Minralogie, l'Eau, les Glaces et l'Activit (OMEGA) instrument (J. Audouard, personal communication). The theoretical maximum resolution is the same as THEMIS, but the nature of the instrument detector (CCD rather than bolometer), the thermal model being used, the timing of the observations, and the process of matching observations to model results are all entirely different. Once cross-referenced, this will hopefully provide a very interesting independent test of the THEMIS technique. However, since OMEGA operates at shorter wavelengths than THEMIS it is only capable of measuring radiation emitted by the surface at relatively high temperatures, necessitating the use of daytime imagery which is more strongly affected by the albedo and topography of the surface.

Chapter 3

METHODS

3.1 Model overview

The problem being approached is essentially one of inverse modeling. Starting from observations of surface temperature, the goal is to calculate surface properties; namely the thickness and TI of a homogeneous layer of soil overlying a homogeneous half-space of bedrock. Both TI and thickness of the layer are obtained by this method concurrently, since from only one observation a thick layer of high-TI material is indistinguishable from a thin layer of lower-TI material. Two observations makes it possible to solve for these two interdependent variables. To this end, two overlapping THEMIS images taken at separate times of year are matched against predicted temperatures from a computational thermal model, and the parameters that most closely match the observed temperatures are chosen. The matching process is done for each pixel in the THEMIS images, producing 100 meter resolution maps of the thickness and TI of the soil layer.

To obtain a predicted surface temperature for Mars from a set of physical parameters, the KRC thermal model is used (Kieffer, 2013). KRC is a one-dimensional, iterative heat-flow model optimized for planetary surfaces, particularly Mars. It requires a number of inputs describing a particular surface including albedo, thermal inertia, and atmospheric parameters such as pressure and opacity, as well as accounting for the latent heat transport caused by the formation and sublimation of carbon dioxide frost on Mars's surface. It produces predicted surface temperatures at fixed times over Mars's entire year, which agree well with both other thermal models and

in-situ observation. It is capable of modeling layered surfaces, but by assumes that each layer is a material of homogenous TI and that the interfaces between layers are flat.

However, the KRC model does not have functionality to do inverse-modeling and produce potential parameters that result in a specific surface temperature. Instead, surface temperatures are produced for varying values of TI and soil layer thickness, and the layer thickness and TI parameters are interpolated to give the closest match to the actual observed temperature. The interpolation significantly complicates the program but also significantly reduces the number of model runs necessary, as well as increasing accuracy and execution speed.

The KRC model takes many other physical properties into account besides the thickness and TI of the upper layer, primarily elevation, the TI of the lower layer, surface albedo, emissivity, slope angle, and atmospheric opacity. These properties must be determined from other data sources. The JMars GIS program (Christensen *et al.*, 2009; Putzig *et al.*, 2005) was used to obtain elevation from the 128-pixel-per-degree (ppd) Mars Orbiter Laser Altimeter (MOLA) global map (Zuber *et al.*, 1992; Smith *et al.*, 2001) and surface albedo from the 8 ppd TES global albedo map (Christensen *et al.*, 2009; Putzig *et al.*, 2005). To estimate atmospheric opacity, an 8 ppd global map of yearly average atmospheric opacity was constructed from TES measurements. Emissivity was fixed at 1.0, and a flat surface was assumed (Bandfield, 2002). The thermal inertia of the lower layer was fixed at 2000, roughly equivalent to basalt or permafrost (Bell, 2008). These "best-guess" values proved to be usable in many cases, due to the relatively small effect these inputs have on surface temperature (see section 3.4).

3.2 Image selection

The goal of this project is to create a targeted survey tool rather than doing in-depth analysis or making global maps, given the necessity of working with archived data and the uncertainty of the quality and reliability of the results. The program is designed to easily and automatically process a large number of human-chosen targets, allowing identification of good candidates for more in-depth analysis.

To this end image selection is entirely automatic and takes a brute-force approach of trying every possible combination of images, relying on the operator to select the best results (see section 3.3). For each target specified in the input file, a KRC model is run to find approximate times of year where the predicted temperature is not cold enough to cause CO_2 frost to form on the surface, and these times of year are excluded from the search. The image metadata database is also checked to ensure that the average temperature of the image is above this threshold. Every night-time THEMIS image that overlaps the target area which passes these tests is retrieved, and every possible combination of image pairs is generated. The simulation-matching process is then run on every image pair.

Only band 9 (12.57 micrometer wavelength) night-time images are used, which are always taken at a local time of approximately 5 a.m. due to the sun-synchronous orbit of the Mars Odyssey spacecraft. The images are calibrated to units of brightness temperature, used as a proxy for the kinetic temperature of the surface. Band 9 is the band generally used for absolute temperature measurement, due to relatively low instrument noise and fewer emissivity variations in the surface, and is least affected by atmospheric dust (Fergason *et al.*, 2006). Only night-time images are used, since day-time temperatures are dominated more by albedo and surface topography than by thermal properties (Christensen *et al.*, 2001; Kieffer *et al.*, 1973, 1977). While the

analysis routine has been tested on day-time images, the glare of sunlight on slopes creates large temperature variations which are not modeled well by the KRC program. Automatically detecting these high temperatures and filtering them out might be an interesting task for future work, since the basic process of model matching against daytime images is otherwise unchanged.

It is an important consideration that the presence of any water or carbon dioxide ice on the surface essentially makes it impossible to find a model solution. As far as the KRC model is concerned Mars's atmosphere starts frosting out onto the surface the instant the temperature drops below the solidification point of CO_2, and starts sublimating when the temperature becomes warm enough again. Though the model keeps track of the amount of frost on the surface and accounts for the mass and energy balance involved, it does not handle kinetic considerations; frost forms and sublimates instantaneously, with the latent heat keeping the surface temperature exactly at the frost point until all the CO_2 ice is gone. This effectively conceals any heat transfer below the surface, keeping it at a fixed temperature regardless of subsurface structure. In reality of course, these processes do not occur instantly, and it is entirely possible to find THEMIS observations with temperatures below (sometimes far below) the freezing point of CO_2, which KRC simply cannot comprehend. Depending on air pressure, the freezing point of CO_2 on Mars varies between roughly 145 and 155 K. A conservative temperature of 160 K is used as a cut-off; any image with an average temperature below this is automatically rejected from consideration. This drastically reduces the number of poor-quality model matches produced.

Once selected and calibrated, the images are projected to a simple cylindrical projection. All images for a particular target point share the same projection frame of reference, allowing them to be easily co-registered and are trimmed down to a 2×2 degree area centered on the target point. Since latitude is an important input to the

KRC model, and the model's latitude is set to that of the target point, straying too far north or south of it will degrade the results (see section 3.4). Since THEMIS images generally take the form of long north-south strips, trimming away the extraneous portions prevents a lot of processor-intensive work on matching models to pixels which, due to differences in latitude, will be necessarily inaccurate. In the end, only one set of model conditions (albedo, elevation, etc) is used for the model match, on the assumption that these properties do not change much over the relatively small area of a THEMIS image.

3.3 Model solution and accuracy

A series of modeled surface temperatures are produced by the KRC program, using the physical parameters obtained from other data sources and values of TI ranging from 50 to 1000 and soil layer thickness ranging from 0 to 1.5 meters, resampled to a uniformly-spaced table of TI and soil layer thickness values. A low-TI soil layer thicker than 1.5 meters effectively insulates any underlying surface from the seasonal heat pulse, so layers thicker than this were not considered. Each combination of TI and layer thickness produces a unique temperature curve; two observed temperatures at midsummer and midwinter are sufficient to constrain a specific set of properties (see Fig. 3.1). Two co-registered THEMIS images taken at different times of year are used to provide these temperatures. The model match is attempted for each pixel in the images, and maps of derived thickness and thermal inertia of the soil layer are produced.

The program will always find the model parameters that best fit the observations, but if the model's assumption are incorrect or the input parameters are particularly poor approximations, the "best fit" may still be very bad. The accuracy of the predicted soil layer TI and thickness depends on the magnitude of the surface

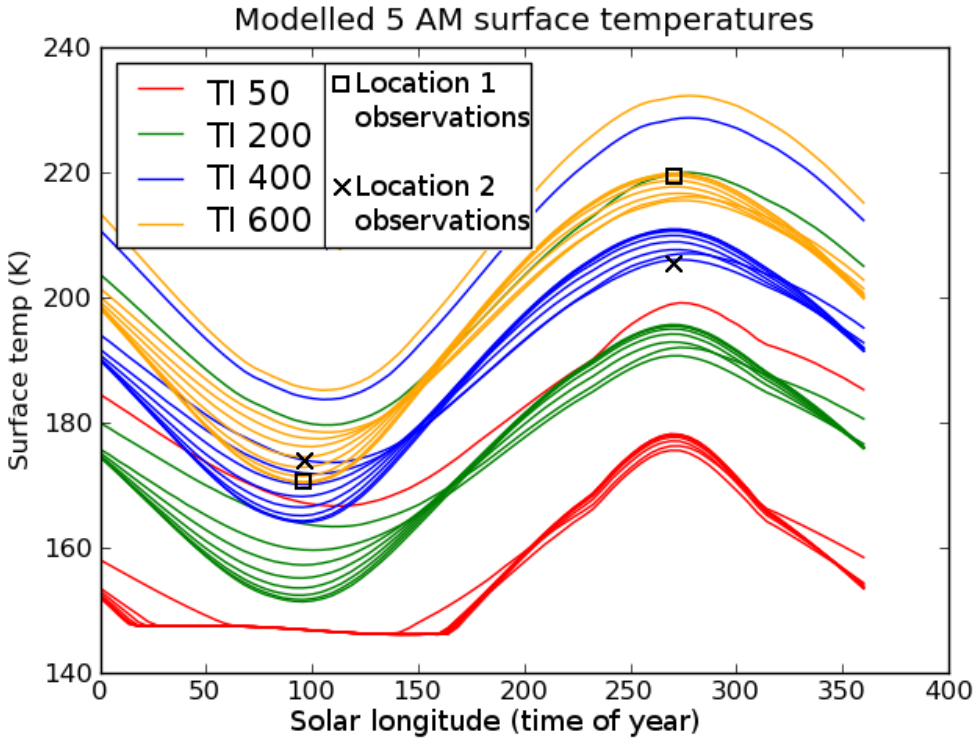

Figure 3.1: Graph showing temperature predictions for different soil layer thicknesses for four different values of TI, for a reference point on Mars's surface (35 degrees N, −2000 meters elevation). The square and cross each represent observed temperatures at a particular location, demonstrating how two observations at different times of year can be used to derive a single unique TI and soil layer thickness.

temperature dependence on those parameters. However, this varies from location to location and season to season. While a particular set of parameters may produce a difference in surface temperature of only a couple degrees near the equator or during spring or fall, it may result in a large temperature difference during summer or winter or at higher latitudes. Essential to interpreting the validity of the results is the ability to check whether the input images are at a location and time of year that should produce large temperature variations. Even if a model is a perfect fit for a pair of observed temperatures, if the difference in temperatures between different sets of TI and layer thickness is only a couple degrees (near the limit of THEMIS's temperature resolution), distinguishing those temperature differences from instrument noise will

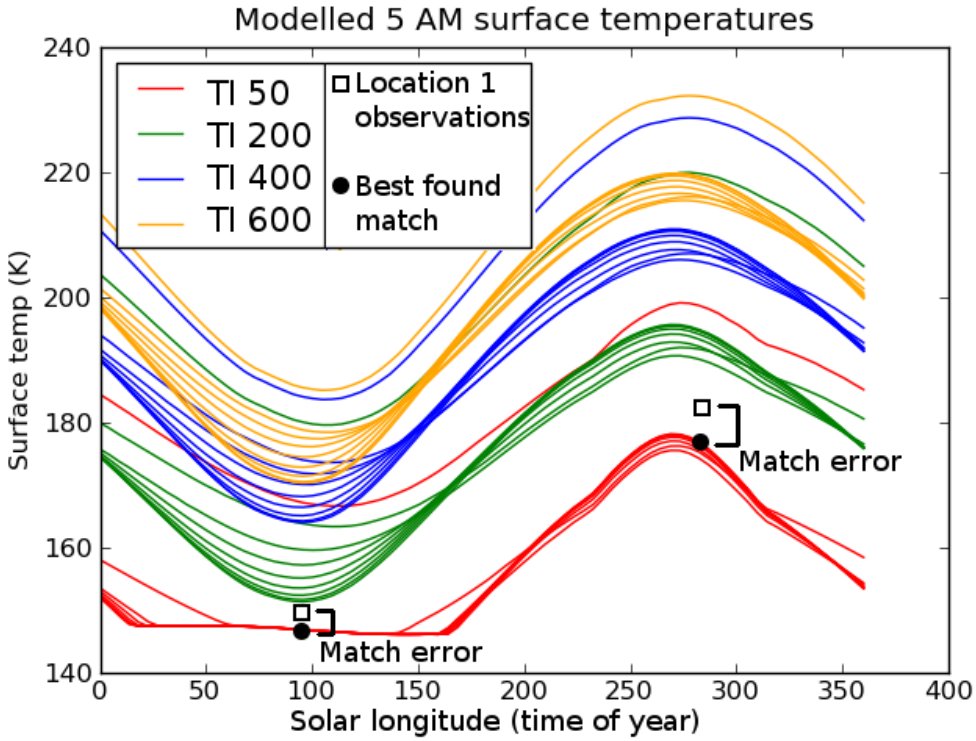

Figure 3.2: Graph showing an example situation where no modeled temperatures fit the observed temperatures. The difference between observed and modeled temperatures is recorded as the match error. The model with the smallest accumulated match error is selected, and a map is produced showing the accumulated match error for each pixel.

be difficult if not impossible. Since a best fit is being found for, on average, several hundred thousand pixels per image pair, it is impractical to try to inspect the results of each match individually, which makes it difficult to manually verify the validity output.

Testing how well the derived TI and layer thickness match the thermal behavior of the surface is done by comparing the modeled surface temperatures for those parameters to the observed temperatures. If the model matches the observations well, the difference between the predicted and observed temperatures will be small or zero. However, if the program could not find a perfect fit the magnitude of the error can be expressed as the accumulated difference between the predicted and observed tem-

peratures for each observation (see Fig. 3.2). The magnitude of the difference may also be informative in determining the cause of the error, combined with a sensitivity analysis (section 3.4). The matching is done per-pixel and a map is produced showing the sum of the temperature errors for each pixel, highlighting areas where the "best fit" model does not match reality very well.

3.4 Sensitivity analysis

To judge the validity of the best-guess model parameters, a sensitivity analysis was performed to discover the magnitude of temperature variation associated with changes in each parameter. Since the KRC model is an iterative physical solution, it is difficult to fully predict the effects of each parameter by analysis: it is not safe to assume that temperature changes linearly with each parameter, and it is not safe to assume that each parameter is independent of others. For instance, the magnitude of the temperature change caused by soil layer thermal inertia varies based on the thickness of the soil layer. If the relationships between these parameters were easy to predict and analyze, an iterative physical model would not be necessary to determine surface temperature

Because of this, a worst-case approach was taken to attempt to determine an upper limit of the temperature effect of each parameter. A set of reference conditions was defined based on average Martian surface properties (Table 3.1), and models were run for these reference conditions in five test "locations" covering a range of latitudes and elevations, recording minimum, maximum and average temperatures at the warmest and coldest times of year. At each test location a set of models was run setting each input parameter individually to reasonable extremes (generally based on the maximum and minimum values found on global maps for that parameter, eg the TES global albedo map for albedo), and the temperatures compared to the reference.

Input parameter	Minimum	Reference conditions	Maximum
Atm. Opacity	0.05	0.1	0.4
Albedo	0.1	0.2	0.3
Latitude	-1°	0	$+1^\circ$
Elevation	-500m	0	$+500$m
Upper layer TI	100	250	600
Lower layer TI	500	2000	2000
Slope North	0°	0°	25°
Slope East	0°	0°	25°
Slope South	0°	0°	25°
Emissivity	0.9	1.0	1.0
Layer thickness	0 m	0 m	1.5 m

Table 3.1: Sensitivity analysis reference conditions tested for each of the five "locations": 50°N at −4250 m elevation, 25°N at −2000 m elevation, on the equator at 0 m elevation, 25°S at 1000 m elevation, and 50°S at 2000 m elevation.

This results in the worst-case sensitivity of surface temperature to variations in the input parameters.

The results demonstrate that night-time surface temperatures are most sensitive to differences in soil layer thickness and thermal inertia, so observations are dominated by those effects. Strong effects are also produced by sunward-facing slopes. Lesser temperature effects are produced by poleward-facing slopes and surface albedo. Small changes in elevation and latitude, eastward or westward facing slopes, lower-layer thermal inertia, surface emissivity, and atmospheric opacity at high latitudes generally result in temperature changes < 2 K, near the limit of THEMIS's temperature resolution. Another problematic factor is that at high latitudes in summer, there may be direct sunlight illuminating and warming the surfaces even during the

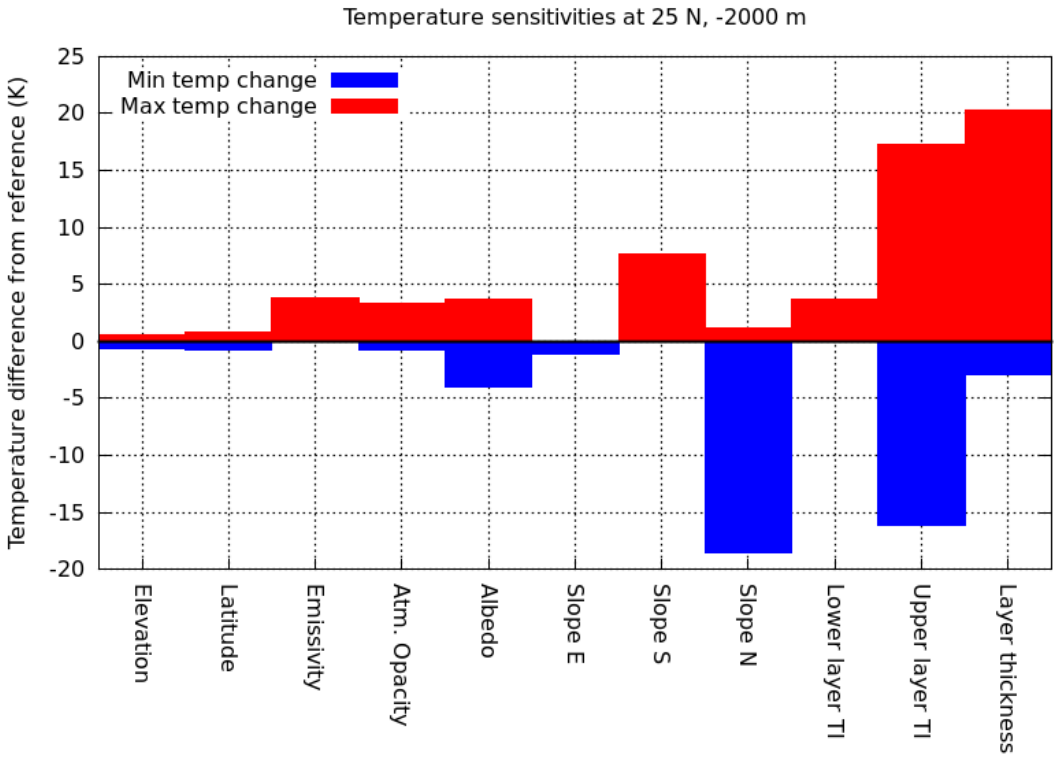

Figure 3.3: Effect of model inputs on predicted surface temperature for a representative location on Mars's surface. Each column is the maximum and minimum difference in surface temperature that was produced by varying the given parameter, compared to a reference surface.

roughly 5 a.m. flyover time of Mars Odyssey. The KRC model accounts for this effect on flat surfaces, but it can cause drastic warming of eastward-facing slopes.

The results of the sensitivity analysis highlights the fact that the derived values for TI and surface layer thickness will be inaccurate on local slopes, and suggests that a more accurate albedo map would also impprove the accuracy of the results. Atmospheric opacity also becomes a more significant effect near the equator. Fortunately, Mars on the whole tends to be low contrast and have little atmospheric dust near the equator. While more accurate model inputs would be desirable, good results can often be produced without them.

The sensitivity analysis also offers a guideline for interpreting temperature errors

from a model match (discussed below), suggesting that above a cutoff of approximately 5 K the error cannot be easily explained by small inaccuracies in input parameters, but that the model's underlying assumptions are likely faulty. For instance, the subsurface may not be well described by a one-dimensional layered model, it may consist of a mixture of materials of different TI's, a high-TI layer overlying a lower-TI one, a tilted contact between the two layers, or other such factors that the KRC model does not account for (Putzig and Mellon, 2007b).

For soil layers thinner than one thermal skin depth, a small temperature error only has a small effect on the derived soil layer thickness and TI, but the detected signal becomes smaller very quickly as the soil layer thickness becomes greater than one skin depth or the thermal inertia approaches that of the underlying bedrock layer. At the reference conditions, for layer thicknesses less than a skin depth a 1 K error in observed temperature equates to approximately 1 cm of layer thickness or 7 units of TI, but these relations increase nonlinearly as soil thickness increases. For this reason the relevant model error should be investigated on a case-by-case basis.

The absolute accuracy of THEMIS is quite good, with a relative precision of about 1.2K and absolute accuracy of 2.8K on a surface of 180K, allowing determination of TI roughly to within 20% (compared to 10-15% for TES) (Fergason *et al.*, 2006). The instrument response has not drifted much over time, so it is fairly safe to compare recent data directly to images taken early in the mission (Christensen *et al.*, 2003; Russell, 2004). One issue that might require further investigation is the possible change of the Martian surface over time due to dust storms. However, even a global dust storm is thought to only remove or deposit a very thin layer of material on the surface (on the scale of a few mm). Such a thin dust layer results in a temperature change at 5 a.m. smaller than THEMIS's temperature resolution, making it effectively invisible, though it may still affect the surface's albedo.

3.5 Slopes

Slope has a potentially large effect on surface temperature, especially at mid latitudes and during seasonal extremes of summer and winter. While slopes facing east or west usually have a minor effect, a southward-facing slope in the northern hemisphere will get much more direct sunlight and hence be much warmer than a flat surface, while a northward facing slope will be much colder. This problem can be divided into two portions, large-scale and local slopes.

Large-scale slopes are long-wavelength changes in topography which are mostly constant within the bounds of a 32-km-by-2-degree THEMIS image segment. Examples would be the north-south hemisphere dichotomy boundary or the flanks of large shield volcanoes. Fortunately, since the slopes in these cases are generally shallow and fairly constant, they tend to have only small effects on surface temperature, and can usually simply be ignored. At worst they will produce a constant temperature offset across the entire image, which will cause an absolute error but preserve relative variations (though subject to the varying resolution of layer thickness). An enhancement to the process would be to use a low-resolution MOLA slope map to find large-scale slopes, and alter the slope input of the model run to match.

Local slopes, such as hills, cliffs, volcanoes, craters and graben, are a much larger problem. Ideally a digital elevation model (DEM) at THEMIS resolution would be obtained either through high-resolution laser altimeter maps or from image stereopairs. However, the global MOLA map is significantly lower-resolution than THEMIS imagery, and stereopair DEM's are not available for the entire surface of Mars. Using a DEM would also mean either performing an additional KRC model run for each pixel in the DEM, or attempting to identify and group areas with a contiguous slope to run one model per slope for the appropriate areas, both of which would significantly

increase the complexity of the program.

In lieu of this, one of the outputs of the process is a simple temperature difference image between the two input images. Local slopes stand out very well in this image, since the sunward side of a hill will be relatively warmer and the lee side will be cooler, producing a visual effect similar to light illuminating the hill. This makes it very easy to see and avoid areas where local slope produces large temperature effects. These areas usually have very high temperature errors as well, and are visible in the temperature error image.

The temperature difference image is also very useful in identifying systemic instrument noise. Some THEMIS images contain vertical or horizontal banding or patterning with variations on the scale of a few degrees K, which may not be completely corrected by the algorithms used in the standard image cleanup. These variations may be nearly invisible in an image, or blend well with terrain features. However, they stand out much more strongly in temperature difference images, making visual identification much easier.

In all cases, elevation changes of > 500 meters within the bounds of the image are going to be problematic due to changes in atmospheric pressure, with a resulting effect on thermal inertia. Currently the only practical solution is to avoid targetting regions with very high vertical relief.

Chapter 4

RESULTS

4.1 Test locations

To test how well the process worked in a diverse set of terrains, a wide variety of locations were targeted, including: spacecraft landing sites, obvious thermal features, and glacier-like forms. Several systematic surveys were also produced, covering a variety of terrains and latitudes. The most interesting results are described below.

Generally, the process worked best in terrains with moderate thermal inertia, smooth surfaces, and in the mid latitudes (see Figure 4.1). Near the equator seasons do not create much temperature variation, resulting in very weak seasonal heat pulses that do not have strong dependence on soil layer thickness; the surface temperature is almost entirely dominated by thermal inertia. However, larger seasonal temperature changes in the southern hemisphere (presumably due to thinner atmosphere) result in stronger signals. While temperature variations based on layers are large enough to be easily distinguishable between 20 and 50 degrees north latitude, similar bounds for the southern hemisphere seem to be between 10 and 50 degrees S.

Further poleward than 50 degrees latitude, CO_2 and water frost, seasonal dust storms, and low temperatures become a significant barrier; seasonal heat pulses are hard to discern simply because the surface is covered with frost for most of the year. Areas with very low thermal inertia, such as Tharsis and Elysium, proved difficult to analyze since the low thermal inertias resulted in very low night-time surface temperatures, and even thin dust layers are very effective at masking the signature of underlying bedrock. There was little noticeable systematic effect of elevation or

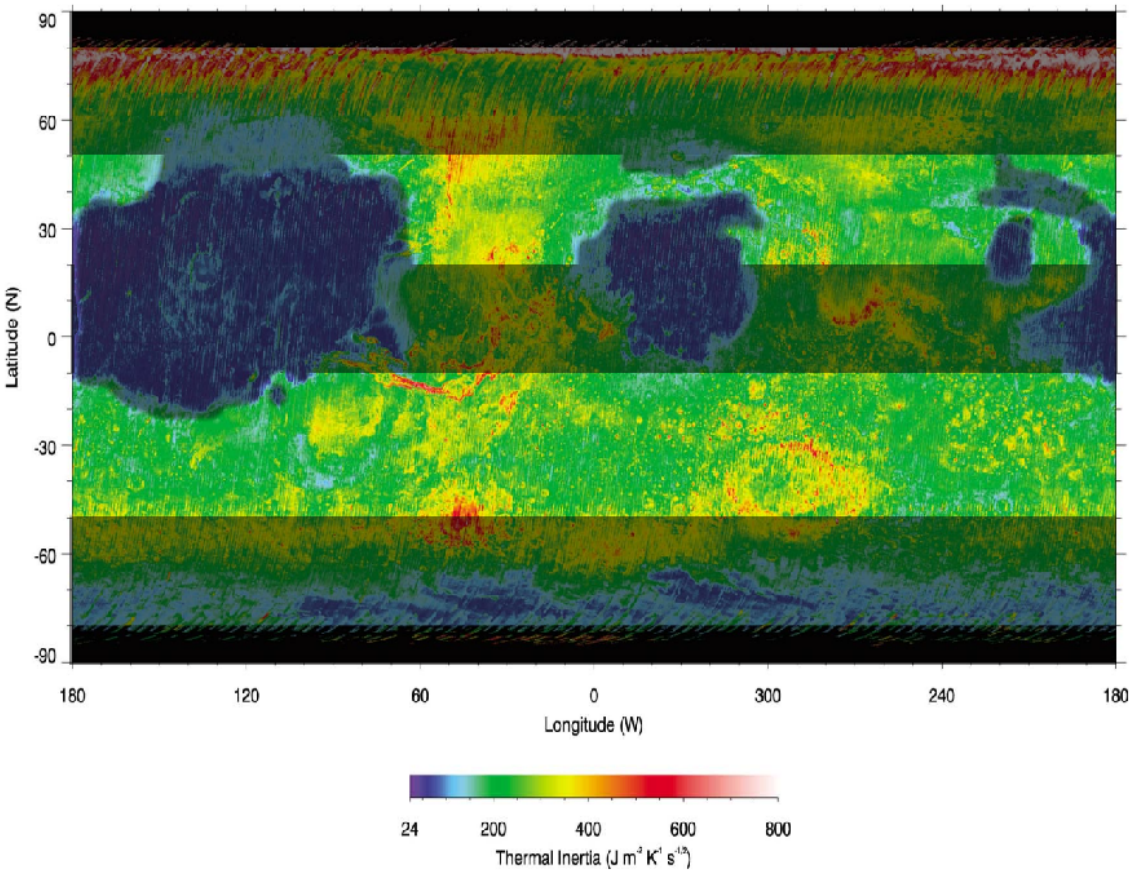

Figure 4.1: Map of Mars, with shaded regions showing approximate area where high latitude or low TI makes it less likely to obtain valid model matches. Base map is TES-derived thermal inertia, from (Putzig *et al.*, 2005).

atmospheric dust (excepting when the elevation change was > 1000 meters or dust significantly degraded the input images), though the southern hemisphere tended to be colder in general, and thus THEMIS night-time images were noisier.

Even outside these ideal locations, it is still possible to produce good model matches, as the following examples will demonstrate. However, beyond these bounds the chances of obtaining a good model match is much more heavily dependent on having high-quality THEMIS images at exactly the right times of year.

Results were double-checked using the Mars Reconnaissance Orbiter Context Camera (CTX), a high-resolution visible-light imager that produces images at up

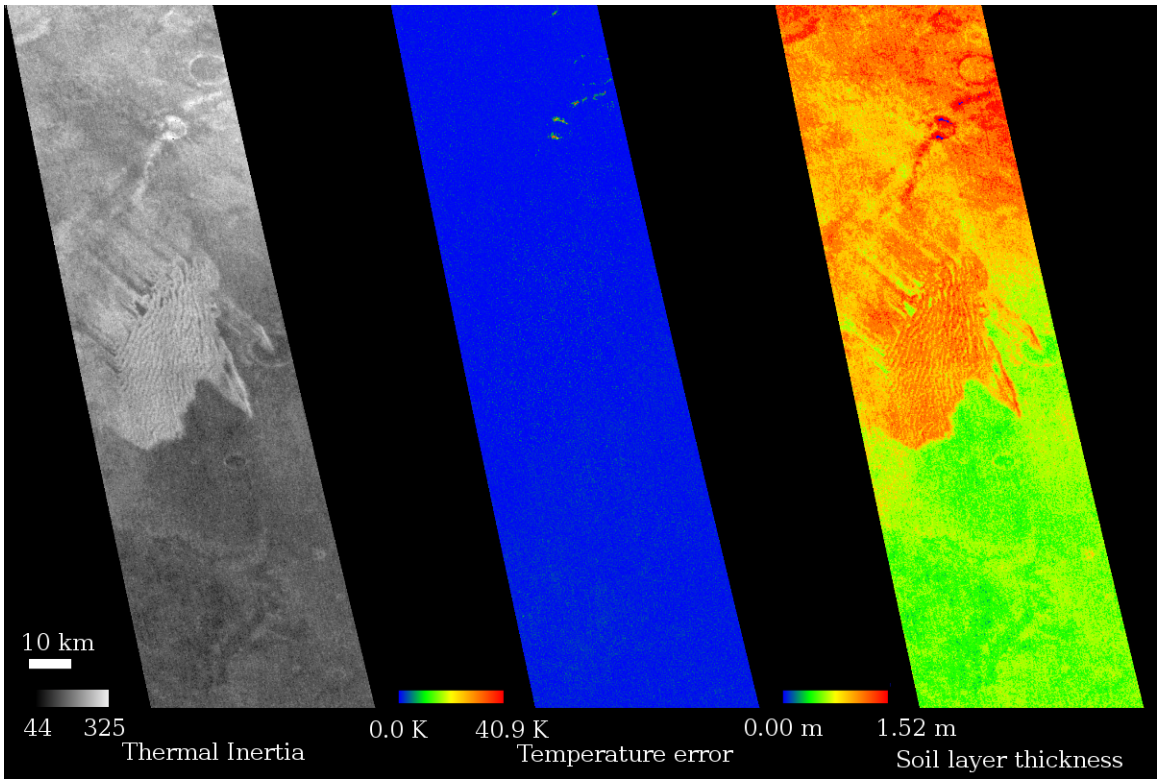

Figure 4.2: Model output for described dune field.

to 3 meters per pixel. This allows qualitative soil cover assessment based on the surface topography, distinguishing rocky terrains from those mantled with dust and sand.

4.2 166 E, 63 S: South-polar dune field

The background field has a TI of about 120, lower than the TES measurement of 150, with the soil layer thickness varying between 15 and 50 cm. The dune field has a TI of roughly 190, again lower than the TES measurement (210). and appear to be transverse dunes with the wind blowing from south-east to north-west in CTX imagery of the area. Further NW of the dunes there is a large, non-dune-forming area with a TI comparable to the dunes, with a soil layer varying from 1 to 1.5 meters thick; the dunes are calculated to be 1.5 meters thick, but are obviously thicker, and

so have simply hit the upper limit of the model's depth resolution. It appears that the area NW of the dunes is covered with sand blown off of them, though much of it does not appear to be a different temperature from the background terrain in most plain THEMIS imagery. There is another non-dune-forming sand-sheet east of the dunes with a similar trail of sand blown off of it. The eastern dune field does not fall within the image, but the sand trails of both are visible: the two can be distinguished separately, with an area of lower soil layer thickness and TI between them where they do not quite intersect.

High-resolution CTX imagery strongly supports this interpretation. The low-TI plain is pervasively covered with dust-devil tracks while the sand sheets are not, and the streams of sand partially or wholly blowing off of the sand sheets conceal the dust-devil tracks. Another possibility is that the region containing dust-devil tracks represents a fairly homogenous, low-albedo surface covered with a very thin layer of high-albedo dust (below the resolution of modeled soil layers), while the region lacking dust-devil tracks is a more heterogenous mixture of high- and low-albedo materials. The region lacking dust-devil tracks matches very well with the thickest modeled soil layers, indicating that the process is indeed detecting regions with substantially different soil structures.

4.3 159.1 E, 9.5 S: Unnamed crater thermal feature

The next target was an old, flat-floored crater approximately 20 km across, henceforth refered to as Crater A (see Figure 4.4. North of Crater A is a unit that is distinctly cooler in THEMIS night-time infrared imagery, and which is interpreted as a low-TI area on the TES TI maps. However, this process indicates that the cool unit is in fact two units, a soil layer 20 cm thick with a TI of roughly 150 lining the northern rim of Crater A, trailing off to a layer approximately 1 cm thick with a TI

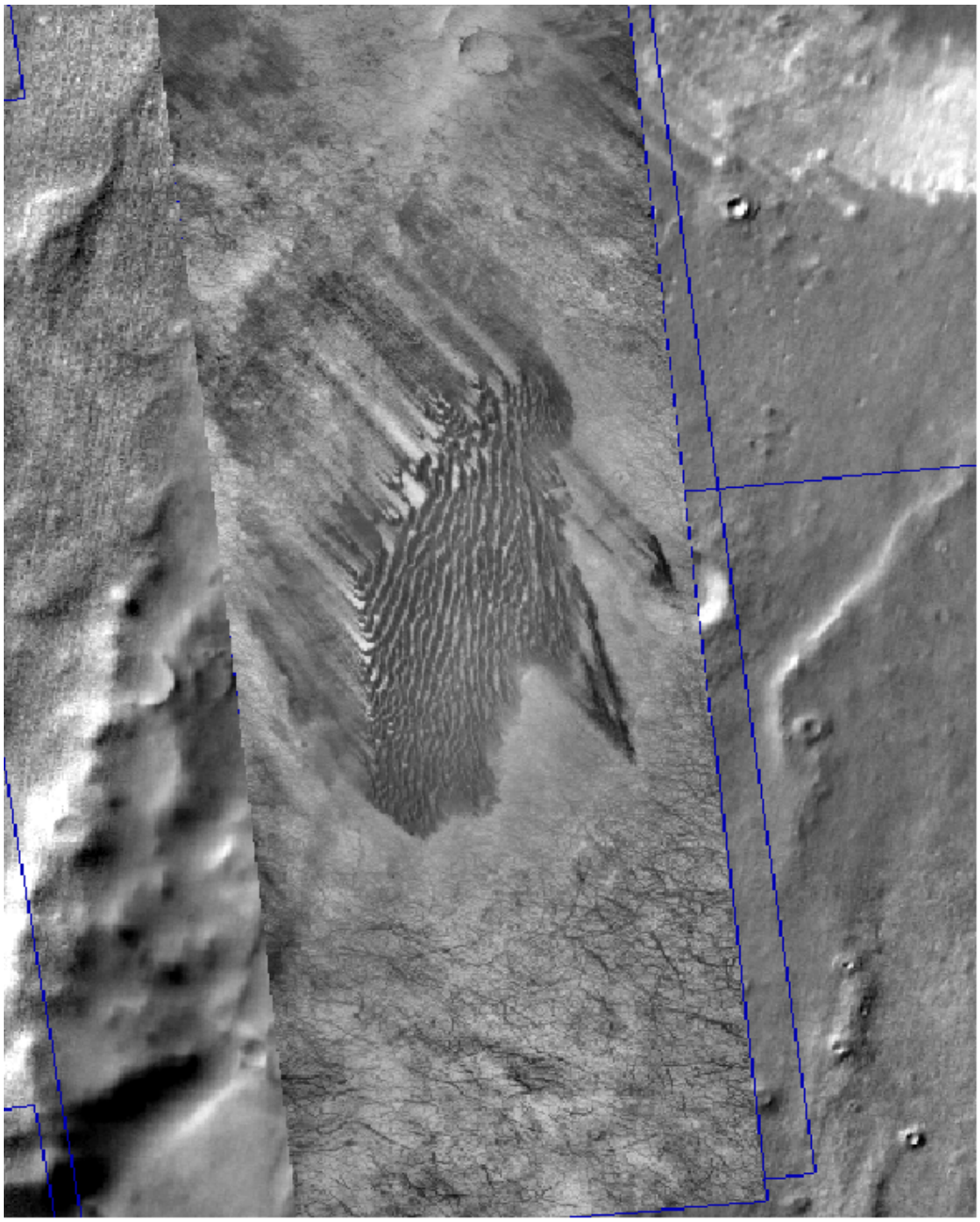

Figure 4.3: CTX visible-light image of dune field overlaid on THEMIS night IR mosaic. The dust-devil tracks south of the dunes are mostly concealed to the north, corresponding to different soil layer thickness and TI units.

of roughly 50 further north (Figure 4.5. These two units are indistinguishable using a non-layered TI measurement, and appear identical in visible light using the Mars Orbiter Camera (MOC) 256 ppd global map. These units are supported by examining high-resolution CTX imagery of the area (Figure 4.6); the terrain in the area with the thicker soil layer is more subdued and rounded, suggesting it is draped with sand or dust, becoming sharper in the area indicated as having a low layer thickness.

Interestingly, approximately 20 km north of the low-thickness layer is a very fresh-looking impact crater roughly 2 km in diameter. It is possible that this crater is recent enough to have been the cause of this change in soil cover thickness, if the wind and shock wave from the impact was strong enough to blow sand and dust away from it, to be piled up against the rim of the larger crater to the south. A more in-depth investigation of this area would be needed to confirm or deny this idea, but the low-temperature area seems interesting enough to be worth the trouble.

4.4 161 E 16 N: Cerberus Fossae

This area is closer to the equator than is ideal, making the effect of soil layer thickness on temperature quite weak. However, several results of even mediocre quality gave very similar results, with fairly thin dust cover layers of 0-20 cm. The warm dust streaks visible in THEMIS daytime images are not apparent, suggesting that they cool down to the ambient temperature of the underlying material before the THEMIS images are taken at roughly 5 am. Thus temperature is controlled mainly by thermal inertia, which averages around 75, agreeing well with the TES TI maps made by (Putzig *et al.*, 2005).

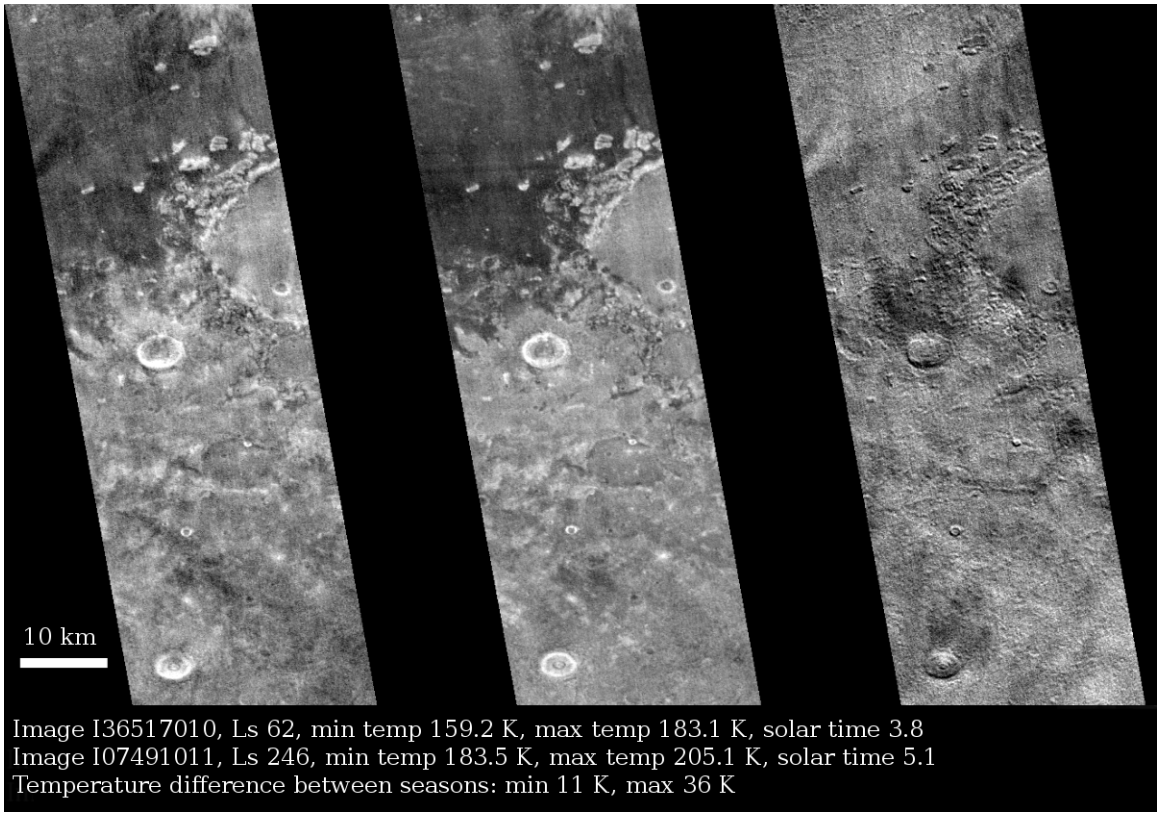

Figure 4.4: Left and center: Night-time THEMIS images of crater A taken at different times of year. Only half the crater is visible in the center-right of each image, approximately 20 km in diameter. Right: Temperature difference between the THEMIS images. Of particular interest is the low-temperature region north of Crater A; see Fig. 4.5.

4.5 67.5 E, 9 N: Nili Patera

This target is worth reporting since it was highlighted in (Fergason *et al.*, 2006) as a probable candidate for sub-surface layering creating visible thermal inertia effects. Unfortunately, according to the KRC model the effects of soil layers at this latitude are predicted to be very small, on the order of 3 K, so it is unlikely for layering alone to be the cause of these TI anomalies. Additionally, this feature is in an area with very low TI (50 or lower) and has up to two kilometers of vertical relief. Because of these factors, this is one of the worst places on Mars to attempt to apply this program. A different data-set or a different method of finding temperature variations (such as

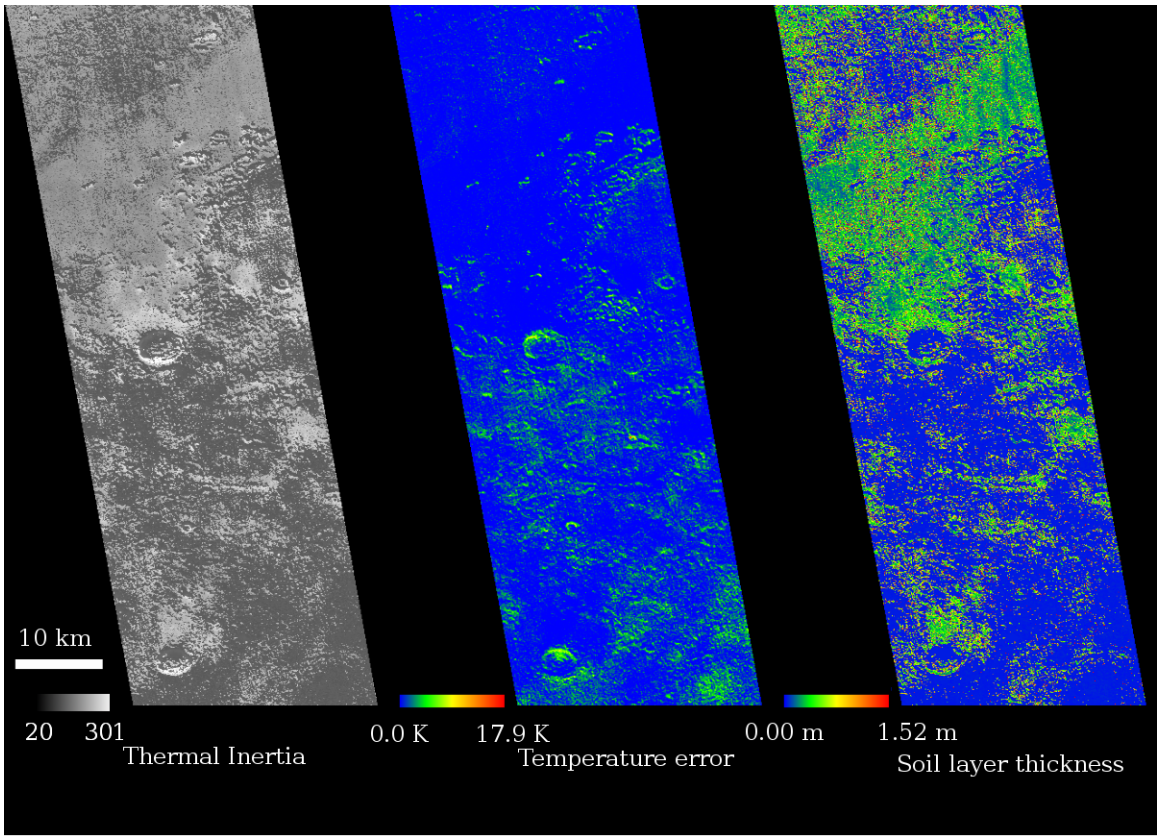

Figure 4.5: Model output from the THEMIS images in Fig. 4.4. The low-temperature region which appeared uniform in THEMIS IR imagery is composed of two units with different TI and soil layer thickness.

looking at different times of day in the same season, using TES or OMEGA data) may prove more fruitful, but using seasonal temperature changes with observations taken at one time of day is unlikely to ever work well.

4.6 Spacecraft landing sites

Unfortunately for these obvious targets no data was obtainable due to technical difficulties further upstream in the THEMIS image handling pipeline. Perhaps in a future work.

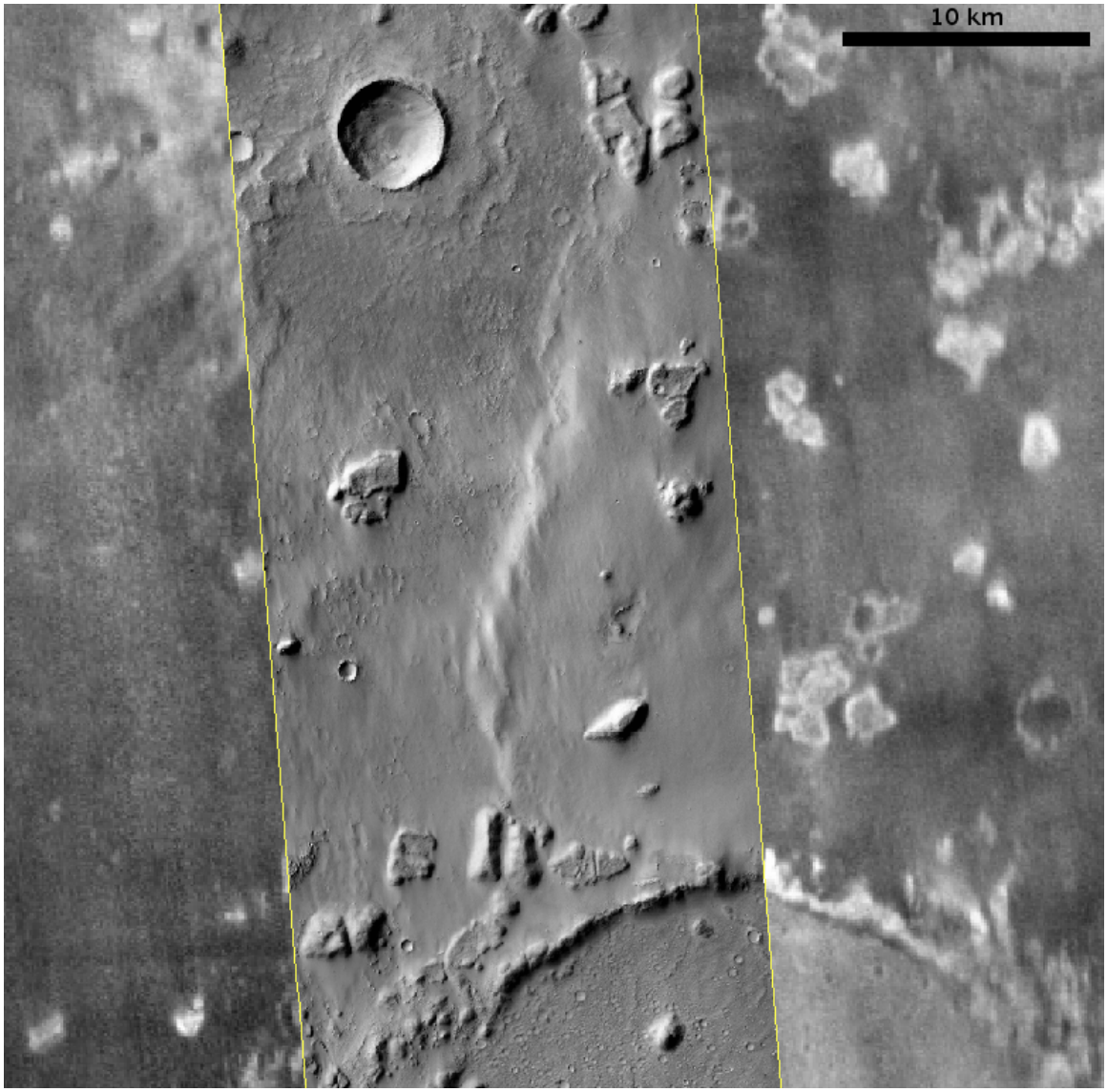

Figure 4.6: CTX visible-light image over THEMIS night IR mosaic of the north edge of Crater A, showing topography with varying definition due to dust cover thickness, and the fresh crater north of it.

Chapter 5

CONCLUSIONS

It is possible to use surface temperature measurements from spacecraft combined with a detailed thermal model to investigate in detail the thermophysical structure of a planet's surface, including subsurface properties down to several thermal skin depths. The THEMIS instrument is capable of providing this data at relatively high spatial resolution, allowing analysis of specific features on a local scale as opposed to previous regional and global-scale maps. The KRC thermal model provides reasonably robust predictions of Mars's surface temperature from a given set of physical parameters, which can be combined with observations to perform inverse modeling to solve for these parameters, particular thermal inertia and soil layer thickness. An analysis program was developed to automatically select all suitable THEMIS data for a target location and perform this analysis on them, capable of running through a large number of targets using archived THEMIS data.

The process of matching a thermal model to observed temperature makes a number of approximations and assumptions, often resulting in a poor model match. The availability of high-quality THEMIS imagery and careful target selection can help increase the reliability of this process, particularly by aiming at strong temperature features in Mars's mid latitudes. Additionally, the validity of a model match can be quantified, allowing poor matches to be identified and discarded. A modeled sensitivity analysis of the influence of various physical parameters on Mars's surface temperature demonstrates that the surface temperatures are dominated by the thickness and thermal inertia of the top meter or two of soil, with steep, small-scale slopes also having a strong influence. The output of the match run includes products to aid

in the identification of local slopes, making it possible to ignore regions where they dominate. However in the end, without direct confirmation from rovers or landers it is difficult to ensure that the assumption of a two-layered surface of homogeneous TI is valid at the scale of a THEMIS pixel.

Despite all this, this process has successfully produced maps of soil thickness assuming a uniform soil over a layer of bedrock or permafrost, with a fair degree of certainty even in unfavorable conditions. These maps have uncovered features that are invisible in simple temperature images, and quantified features that are apparent but difficult to measure in visible light images. Thus it will hopefully be useful as a supporting resource for investigating specific features with a strong thermal signature, or as a survey tool to attempt to perform rough analysis on a large number of landforms. It should be particularly useful when aimed at features which have a strong thermal component or which are thought to be created by near-surface ice, such as polygonal terrains and glacier-like forms.

Chapter 6

FUTURE WORK

6.1 Targeted observations

This technique is only as accurate as its input data, and despite THEMIS's extensive image archive, large areas of Mars are only poorly covered by high-quality, high-resolution thermal images. Whether or not an arbitrary place on its surface has high-quality night-time imagery taken during appropriate seasons involves an element of luck. Fortunately, THEMIS and Mars Odyssey are still operational, so it is possible to request new imagery of specific regions. However the requirement of multiple images taken at widely-separated seasons, combined with Mars's long year, means that obtaining new data specifically for this project is a long-term endeavor (though a potentially fruitful source of targets may be to search the THEMIS ROI list for existing targets marked for repeated observations).

Twenty-one regions-of-interest (ROI's) were submitted to the THEMIS mission planning team in February 2013, labeled for repeated observations each time the Mars Odyssey spacecraft flies over them (approximately once every six weeks). A variety of different terrains were targeted, including several polygonal terrains and sand sheets, crater ejecta, lava flows, glacier-like forms, and the edge of the Tharsis low-TI region. THEMIS visible light observations were also requested, potentially allowing quantitative albedo maps to be made, or at least offering confirmation that there have been no major changes in dust cover between observations based on morphology and albedo. Hopefully observation of these targets will cover the full extent of an entire Martian year, allowing these regions to be studied in much greater detail and

with more precision. Some regions such as the sand sheets have physical features that should let us measure the soil layer thickness via other methods (ie high-resolution visible-light imagery), allowing independent confirmation of the results for those areas.

6.2 Model architecture

In the end, the targeted-survey method was not as useful as it was hoped. The assumption is that one set of model inputs (elevation, albedo, etc) would be used per survey site, thus simplifying processing and making individual areas easier to understand. However, even with the relatively small areas covered by single THEMIS images, surface conditions change enough to make multiple sets of model inputs desirable; this single-model assumption was more of a hindrance than help. This architecture also results in more difficulty in observing a larger area. The seasonal dependence of the images makes binning and mosaicking more challenging, but the ability to make regional maps would be very useful. Though it would be more complicated and much more computationally intensive, the more traditional method of creating a large mosaic and finding a solution for each pixel (or small multi-pixel chunks such as THEMIS framelets, as in (Fergason *et al.*, 2006)) may be more fruitful in the future.

REFERENCES

Bandfield, J. L., "Global mineral distributions on Mars", Journal of Geophysical Research: Planets **107**, E6, 9–1–9–20, URL http://dx.doi.org/10.1029/2001JE001510 (2002).

Bandfield, J. L., "High-resolution subsurface water-ice distributions on Mars", Nature **447**, 7140, 64–67, URL http://dx.doi.org/10.1038/nature05781 (2007).

Bandfield, J. L. and W. C. Feldman, "Martian high latitude permafrost depth and surface cover thermal inertia distributions", Journal of Geophysical Research: Planets **113**, E8, URL http://dx.doi.org/10.1029/2007JE003007 (2008).

Bell, J., ed., *The Martian Surface: Composition, Mineralogy and Physical Properties* (Cambridge University Press, 2008).

Betts, B. H., B. C. Murray and T. Svítek, "Thermal inertias in the upper millimeters of the Martian surface derived using Phobos' shadow", Journal of Geophysical Research: Planets **100**, E3, 5285–5296, URL http://dx.doi.org/10.1029/95JE00226 (1995).

C., J. and Price, "On the analysis of thermal infrared imagery: The limited utility of apparent thermal inertia", Remote Sensing of Environment **18**, 1, 59 – 73, URL http://www.sciencedirect.com/science/article/pii/0034425785900380 (1985).

Chase, S. C., J. L. Engel, H. W. Eyerly, H. H. Kieffer, F. D. Palluconi and D. Schofield, "Viking infrared thermal mapper", Appl. Opt. **17**, 8, 1243–1251, URL http://ao.osa.org/abstract.cfm?URI=ao-17-8-1243 (1978).

Christensen, P. R., "The spatial distribution of rocks on Mars", Icarus **68**, 2, 217 – 238, URL http://www.sciencedirect.com/science/article/pii/0019103586900205 (1986).

Christensen, P. R., D. L. Anderson, S. C. Chase, R. N. Clark, H. H. Kieffer, M. C. Malin, J. C. Pearl, J. Carpenter, N. Bandiera, F. G. Brown and S. Silverman, "Thermal emission spectrometer experiment: Mars observer mission", Journal of Geophysical Research: Planets **97**, E5, 7719–7734, URL http://dx.doi.org/10.1029/92JE00453 (1992).

Christensen, P. R., J. L. Bandfield, J. F. Bell III, N. Gorelick, V. E. Hamilton, A. Ivanov, B. M. Jakosky, H. H. Kieffer, M. D. Lane, M. C. Malin, T. McConnochie, A. S. McEwen, H. Y. McSween, G. L. Mehall, J. E. Moersch, K. H. Nealson, J. W. Rice, M. I. Richardson, S. W. Ruff, M. D. Smith, T. N. Titus and M. B. Wyatt, "Morphology and Composition of the Surface of Mars: Mars Odyssey THEMIS Results", Science **300**, 5628, 2056–2061, URL http://www.sciencemag.org/content/300/5628/2056.abstract (2003).

Christensen, P. R., J. L. Bandfield, V. E. Hamilton, S. W. Ruff, H. H. Kieffer, T. N. Titus, M. C. Malin, R. V. Morris, M. D. Lane, R. L. Clark, B. M. Jakosky, M. T. Mellon, J. C. Pearl, B. J. Conrath, M. D. Smith, R. T. Clancy, R. O. Kuzmin, T. Roush, G. L. Mehall, N. Gorelick, K. Bender, K. Murray, S. Dason, E. Greene, S. Silverman and M. Greenfield, "Mars Global Surveyor Thermal Emission Spectrometer experiment: Investigation description and surface science results", Journal of Geophysical Research: Planets **106**, E10, 23823–23871, URL http://dx.doi.org/10.1029/2000JE001370 (2001).

Christensen, P. R., E. Engle, S. Anwar, S. Dickenshied, D. Noss, N. Gorelick and M. Weiss-Malik, "JMARS - A Planetary GIS", AGU Fall Meeting Abstracts p. A6 (2009).

Feldman, W. C., M. T. Mellon, O. Gasnault, B. Diez, R. C. Elphic, J. J. Hagerty, D. J. Lawrence, S. Maurice and T. H. Prettyman, "Vertical distribution of hydrogen at high northern latitudes on Mars: The Mars Odyssey Neutron Spectrometer", Geophys. Res. Lett. **34**, 5, L05201, URL http://dx.doi.org/10.1029/2006GL028936 (2007).

Fergason, R. L., P. R. Christensen and H. H. Kieffer, "High-resolution thermal inertia derived from the Thermal Emission Imaging System (THEMIS): Thermal model and applications", J. Geophys. Res. **111**, E12, E12004, URL http://dx.doi.org/10.1029/2006JE002735 (2006).

Kieffer, H. H., "Thermal model for analysis of Mars infrared mapping", Journal of Geophysical Research (2013).

Kieffer, H. H., S. C. Chase, E. Miner, G. Münch and G. Neugebauer, "Preliminary report on infrared radiometric measurements from the Mariner 9 spacecraft", Journal of Geophysical Research **78**, 20, 4291–4312, URL http://dx.doi.org/10.1029/JB078i020p04291 (1973).

Kieffer, H. H., S. C. Chase, E. D. Miner, F. D. Palluconi, G. Münch, G. Neugebauer and T. Z. Martin, "Infrared Thermal Mapping of the Martian Surface and Atmosphere: First Results", Science **193**, 4255, 780–786, URL http://www.sciencemag.org/content/193/4255/780.abstract (1976).

Kieffer, H. H., T. Z. Martin, A. R. Peterfreund, B. M. Jakosky, E. D. Miner and F. D. Palluconi, "Thermal and albedo mapping of Mars during the Viking primary mission", Journal of Geophysical Research **82**, 28, 4249–4291, URL http://dx.doi.org/10.1029/JS082i028p04249 (1977).

Mellon, M. T. and B. M. Jakosky, "The distribution and behavior of Martian ground ice during past and present epochs", J. Geophys. Res. **100**, E6, 11781–11799, URL http://dx.doi.org/10.1029/95JE01027 (1995).

Mellon, M. T., B. M. Jakosky and S. E. Postawko, "The persistence of equatorial ground ice on mars", J. Geophys. Res. **102**, E8, 19357–19369, URL http://dx.doi.org/10.1029/97JE01346 (1997).

Morrison, D., C. Sagan and J. B. Pollack, "Martian temperatures and thermal properties", Icarus **11**, 1, 36 – 45, URL http://www.sciencedirect.com/science/article/pii/0019103569901134 (1969).

Neugebauer, G., G. Münch, H. Kieffer, S. C. Chase, Jr. and E. Miner, "Mariner 1969 Infrared Radiometer Results: Temperatures and Thermal Properties of the Martian Surface", Astronomical Journal **76**, 719 (1971).

Palluconi, F. D. and H. H. Kieffer, "Thermal inertia mapping of Mars from 60°S to 60°N", Icarus **45**, 2, 415–426, URL http://www.sciencedirect.com/science/article/pii/0019103581900440 (1981).

Presley, M. A. and P. R. Christensen, "The effect of bulk density and particle size sorting on the thermal conductivity of particulate materials under martian atmospheric pressures", Journal of Geophysical Research: Planets **102**, E4, 9221–9229, URL http://dx.doi.org/10.1029/97JE00271 (1997a).

Presley, M. A. and P. R. Christensen, "Thermal conductivity measurements of particulate materials 1. A review", Journal of Geophysical Research: Planets **102**, E3, 6535–6549, URL http://dx.doi.org/10.1029/96JE03302 (1997b).

Presley, M. A. and P. R. Christensen, "Thermal conductivity measurements of particulate materials 2. Results", Journal of Geophysical Research: Planets **102**, E3, 6551–6566, URL http://dx.doi.org/10.1029/96JE03303 (1997c).

Putzig, N. E. and M. T. Mellon, "Apparent thermal inertia and the surface heterogeneity of mars", Icarus **191**, 1, 68 – 94, URL http://www.sciencedirect.com/science/article/pii/S001910350700231X (2007a).

Putzig, N. E. and M. T. Mellon, "Thermal behavior of horizontally mixed surfaces on Mars", Icarus **191**, 1, 52 – 67, URL http://www.sciencedirect.com/science/article/pii/S0019103507001339 (2007b).

Putzig, N. E., M. T. Mellon, K. A. Kretke and R. E. Arvidson, "Global thermal inertia and surface properties of Mars from the MGS mapping mission", Icarus **173**, 2, 325 – 341, URL http://www.sciencedirect.com/science/article/pii/S0019103504002957 (2005).

Russell, C. T., ed., *The Thermal Emission Imaging System (THEMIS) for the Mars 2001 Odyssey Mission* (Springer Netherlands, 2004), URL http://dx.doi.org/10.1007/978-0-306-48600-5_3.

Sizemore, H. G., M. T. Mellon and M. P. Golombek, "Ice table depth variability near small rocks at the Phoenix landing site, Mars: A pre-landing assessment", Icarus **199**, 2, 303 – 309, URL

http://www.sciencedirect.com/science/article/pii/S0019103508003710 (2009).

Smith, D. E., M. T. Zuber, H. V. Frey, J. B. Garvin, J. W. Head, D. O. Muhleman, G. H. Pettengill, R. J. Phillips, S. C. Solomon, H. J. Zwally, W. B. Banerdt, T. C. Duxbury, M. P. Golombek, F. G. Lemoine, G. A. Neumann, D. D. Rowlands, O. Aharonson, P. G. Ford, A. B. Ivanov, C. L. Johnson, P. J. McGovern, J. B. Abshire, R. S. Afzal and X. Sun, "Mars Orbiter Laser Altimeter: Experiment summary after the first year of global mapping of Mars", Journal of Geophysical Research: Planets **106**, E10, 23689–23722, URL http://dx.doi.org/10.1029/2000JE001364 (2001).

Wechsler, A. E. and P. E. Glaser, "Pressure effects on postulated lunar materials", Icarus **4**, 4, 335–352, URL http://www.sciencedirect.com/science/article/pii/0019103565900382 (1965).

Zuber, M. T., D. E. Smith, S. C. Solomon, D. O. Muhleman, J. W. Head, J. B. Garvin, J. B. Abshire and J. L. Bufton, "The Mars Observer laser altimeter investigation", Journal of Geophysical Research: Planets **97**, E5, 7781–7797, URL http://dx.doi.org/10.1029/92JE00341 (1992).